Electronic Letters on Computer Vision and Image Analysis 23(1):47-59, 2024

Classification of radiological patterns of tuberculosis with a Convolutional neural network in x-ray images

Jessica Sanchez *, Adrian Trueba *, Jair Cervantes *, Farid Garcia-Lamont, José Sergio Ruiz Castilla*, and Karthik Kantipudi+

* *UAEMEX (Autonomous University of Mexico State), Texcoco, 56259, Mexico*
+*National Institutes of Health, Bethesda, MD, USA*

Received 9th of March, 2023; accepted 8th of June 2024

Abstract

Tuberculosis is a disease that causes more deaths worldwide. To detect it, laboratory studies are performed so it can take more than 30 days, the quickest diagnosis is made by X-ray radiographs. Tuberculosis presents different radiological patterns (consolidation, fibrosis, opacity, pleural, nodules and cavitations), depending on the pattern found, the specialist prescribes the most appropriate treatment. According to the diagnosis and radiographs provided by the National Institute of Allergy and Infectious Disease laboratory, there is not only one single pattern in a radiograph, but there can also be from one to six patterns. The aim of this article is to detect the presence of two to six tuberculosis patterns in the same X-ray radiograph. No research was found that addresses the classification of more than one pattern of tuberculosis, this is what is relevant to this work.. For tuberculosis pattern classification, a convolutional neural network with its own architecture was proposed, and the VGG16, InceptionV3 and ResNet-50 architectures were tested. A support vector machine was used for multi-classification. The results were validated with the area under the curve, with the Macro-averange metric with the following results: in the proposed architecture and the InceptionV3 it was 0.80, and in the VGG16 it was 0.75, as for the ResNet-50 network 0.79 was obtained. The proposed architecture has better classification results, as does InceptionV3.

Key Words: Tuberculosis patterns, Chest X-rays, convolutional neural networks.

1 Introduction

One disease that has not been eradicated in the world is tuberculosis (TB), an infectious bacterial infection caused by the bacterium Mycobacterium or Koch's bacillus [1] . Although it is curable and preventable, it still causes deaths because it is spread through the air; when a person with pulmonary TB coughs or sneezes, they expel tubercle bacilli into the air and spread the disease [2].

The World Health Organization (WHO) estimates that one third of the world's population has latent TB, meaning that there are people infected with the bacillus who have no symptoms of the disease, but are carriers of the bacillus and can transmit the infection [3]. People infected with the TB bacillus have a 5-10 %. lifetime

Correspondence to: jsancheza560@alumno.uaemex.mx

Recommended for acceptance by Angel D. Sappa
https://doi.org/10.5565/rev/elcvia.1822
ELCVIA ISSN:1577-5097
Published by Computer Vision Center / Universitat Autònoma de Barcelona, Barcelona, Spain

risk of developing the disease [4]. Since 2015, the WHO has been implementing a protocol to reduce the number of people infected with the disease, which requires rapid and accurate diagnosis by doctors so that patients can start treatment as soon as possible to avoid infecting others, and the patient can begin to be cured [5].

Studies [6, 7, 8] have shown that chest radiographs (X-rays) have been used by medical experts to detect and diagnose COVID-19, tuberculosis and pneumonia.

When diagnosing tuberculosis in a chest X-ray, it is important to consider that the bacillus can attack several areas and grow in colonies or clusters, which can be observed in the X-ray forming different structures, depending on the structure a pattern is formed in which the following stand out: consolidation, fibrosis, opacity, pleural, nodules and cavities. This is important because depending on the pattern formed, a treatment is prescribed.

It is worth noting that more than one pattern can be found simultaneously in the same patient, this was found in the set of images provided by the National Institute of Allergy and Infectious Diseases (NIAID) TB Portals DEPOT [9]. This is important because two to six related patterns can be found in the same patient.

The contribution of this study is the classification of the association of tuberculosis patterns in radiographs of contaminated patients using CNN. It should be noted that no studies have been found on this line of research; those consulted classify only a single pattern in radiographs, whereas in reality there are two to six associated patterns.

CNNs are used for image classification where patterns are detected, the more images used the better. There are several CNN architectures that have a margin of error, their training is done with very large datasets. In this work we have a dataset of 450 images per class, so it was decided to create our own architecture, based on the number of images available, three networks were also used; InceptionV3, (c) VGG16 and (d) ResNet50 to have a point of comparison with the performance of the proposed network, the selected CNNs have shown good results in other works [6, 10, 11].

The article is structured as follows: section 2 reviews the state of the art, section 3 describes the proposed method, materials and methodology, section 4 presents the results and discussion, and the conclusions and acknowledgements are presented at the end.

2 Related works

The following experiment [12] used three databases (Montgomery, Shenzhen, Belarus TB) with a total of 1,007 images. These were systematised in a 256 x 256 matrix and two deep neural networks (AlexNet and GoogLeNet) were used; an AUC of 0.99 %. and a sensitivity of 97.3 % were obtained. It is noteworthy that the authors mention three patterns of tuberculosis (pleural, miliary and with cavitations), but in the conclusions of the paper they only comment on the classification of normal and tuberculous classes, without mentioning the specific findings of arrest for each of the patterns on the radiographs.

In [13] they evaluated the feasibility of detecting and classifying tuberculosis patterns based on deep learning. The experiment consists of obtaining a photograph of a radiograph, analysing the photograph with a deep network and classifying it into the following classes: cavity, consolidation, effusion, bowel changes, miliary pattern or normal examination. The classification was evaluated by analysing the characteristics of each pattern to be identified, giving an AUC of 0.82%.

In another study [14], chest radiographs are used to detect tuberculosis using radiological patterns with convolutional neural networks (Faster RCNN, EPN and a proprietary neural network) considering the patterns; free pleural, miliary, encapsulated pleural, nodules, calcification and exudation. The results show the accuracy of identifying each of the patterns. The best identified pattern is miliary with 87.72 % using the FPN method. The identification of the other patterns ranged from 0.37% to 64.92%, which shows that the identification of tuberculosis by pattern is a research challenge. It is noteworthy that this work has the virtue of considering patterns of tuberculosis. This is essential, as the detection of tuberculosis patterns allows a specific treatment to be determined in order to treat the disease effectively.

In [15] it is mentioned that tuberculosis is still an urgent problem, especially in low-income countries. Therefore, they propose to develop a convolutional neural network that can provide a reliable diagnosis by using a mobile phone to capture the x-ray and display the diagnosis on it, in order to provide a faster pre-diagnosis.

The following study [16] proposes an automatic TB detection system using advanced deep learning (DL) models. In the experiments, they used different convolutional neural network (CNN) models and compared the classification using three publicly available CXR datasets. EfficientNetB3, one of the CNN models, achieves the highest accuracy of 99.1 %, with a receiver operating characteristic of 99.9 % and an average accuracy of 98.7 %.

In this research [17] , they present a novel TB-UNet, which is based on the dilated fusion block and the attention block for accurate (0.9574) segmentation of lung regions. They also propose TB-DenseNet, which is based on five dual convolution blocks, a DenseNet-169 layer and a feature fusion block for accurate classification of TB images.

This study [18] aimed to develop a TB detection model using chest X-ray images obtained from datasets on Kaggle.com. A dataset of over 1196 chest X-ray images, including 633 TB-positive chest X-rays and 563 normal cases, was utilized for model development. The TB detection model developed using Google's Collaboration Platform. The model achieved an area under the curve (AUC) of 0.934, indicating its ability to accurately classify TB positive and normal chest X-ray images. Furthermore, the overall accuracy of the model was determined to be 94%.

In another experiment [19], the WSODTL-TBC model was tested using a data set from the Kaggle repository. The dataset contains a total of 4200 images, with 3500 images from the Normal class and 700 images from the TB class. The results implied that the WSODTL-TBC model showed effective results. The WSODTL-TBC model has provided an accuracy of over 98.9 %. While the VGG-16, VGG-19, Inception-v3, Xception and AlexNet models have achieved a lower accuracy of 86.26 %, 92.39 %, 91.06%, 87.65% and 92.30% respectively.

This paper proposes a method to classify more than one pattern of tuberculosis in a single chest X-ray using a deep convolutional neural network to help an inexperienced physician detect this disease and make a correct diagnostic decision, no evidence of similar work was found.

3 Proposed Method

The diagram in figure 1 shows the methodology proposed for the development of the project. Using the database of radiographic images provided by the laboratory of the National Institute of Allergy and Infectious Diseases, the images were classified according to the patterns found in each radiograph, and stored in 6 folders (table 1). The size of the radiographs was then homogenised to 256*256 and the data normalised (0.1).

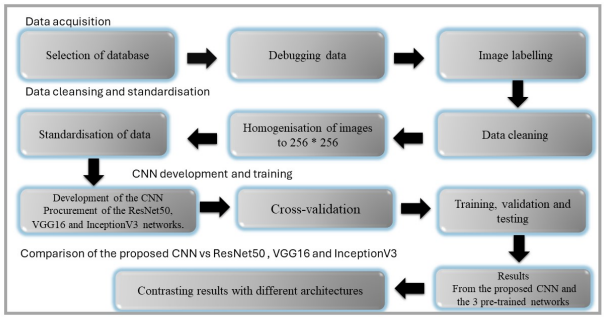

Figure 1: Proposed methodology

3.1 Materials and Methods

”Data were obtained from the TB Portals (https://tbportals.niaid.nih.gov), an open-access TB data resource supported by the National Institute of Allergy and Infectious Diseases (NIAID) Office of Cyber Infrastructure and Computational Biology (OCICB) in Bethesda, MD. These data were collected and submitted by members of the TB Portals Consortium (https://tbportals.niaid.nih.gov/Partners). Investigators and other data contributors who originally submitted the data to the TB Portals were not involved in the design or analysis of this study.

The images were divided into folders for training and validation. Training and validation were performed. Finally, the results were compared.

It is important to mention that the images provided by the NIAID were diagnosed by experts; they only mention how many and which patterns were found in each x-ray, without identifying each of the patterns in the tuberculosis x-rays. In the investigation, 1687 radiographs were selected, which were labeled into classes, as shown in Table 1.

Number of patterns	Pattern combination	Images	Class
No patterns	Healthy	500	0
2 patterns	Consolidation and opacity	122	2
3 patterns	Fibrosis, opacity and nodules	220	3
4 patterns	Consolidation, fibrosis, opacity and nodules	491	4
5 patterns	Consolidation, fibrosis, opacity, nodules and cavitations	480	5
6 patterns	Consolidation, fibrosis, opacity, pleural, nodules and cavitations	154	1

Table 1: Tuberculosis patterns found in radiographs and definition of classes to be classified

3.1.1 Data cleansing and normalization

The images were stored in six folders based on the number of patterns, which determined the classes for classification. The images were balanced to ensure equal numbers, preventing any bias in the results, with each category adjusted to 450 images. Tuning was carried out using the Keras API Data Augmentation function. Given the varying resolutions of the images, a uniform size of $256x256$ was achieved using the Keras API.

The images were divided into three groups; the first was for training with 283 images, the second had 122 for validation, and the last one with 45 for the tests. The assignment of the images was done randomly in each folder.

For the normalisation of the data, the value of the pixels was divided by 255 to obtain values between $0$and 1; this procedure was carried out using the ImageDataGenerator function of the Keras API.

The training was carried out with a PC with a Core i9, 10th generation, with 16 GB RAM and 240 GB solid-state drive. It was trained with a 10 core cpu x64.

The convolutional neural network was programmed with Python, using the machine learning libraries: TensorFlow, Scikit-Learn, NumPy, and Pandas.

For the selection of images, it was carried out using $flow_from_directory$ function of the Keras API, which labelled the 6 classes, considering each class (0 = healthy, 1 = Patterns 6, 2 = Patterns 2, 3 = Patterns 3, 4 = Patterns 4, 5 = Patterns 5). As shown in Figure 2.

3.1.2 CNN development and training

The convolutional neural network was programmed with Python, using the machine learning libraries: TensorFlow, Scikit-Learn, NumPy, and Pandas. A CNN was designed and proposed, and other pre-trained networks such as ResNet50, VGG16 and InceptionV3 were also used.

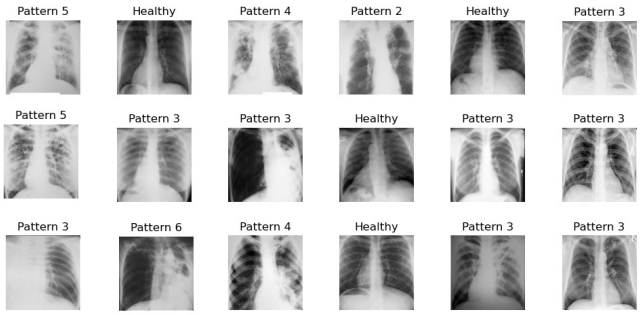

Figure 2: Selection of radiographs for training, validation and testing

3.2 Proposed architecture

After testing several topologies for the classification of the six classes, the proposed CNN is the one that obtained the best results, as shown in Figure 3 . In each layer, the Dropout function was used to prevent the network from memorising and perform a better classification, as it randomly disconnects neurons, and the MaxPooling function was also used to reduce the output characteristics. An SVM was programmed to perform the classification, which has been shown to be efficient in other research [20, 21]. Input layer [22]: x^l in the

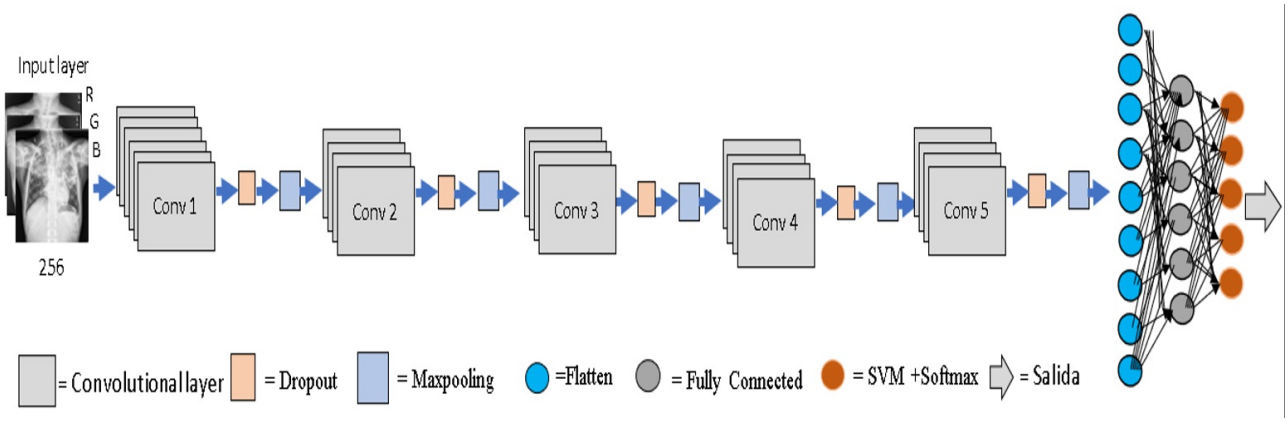

Figure 3: Network architecture used

form of a 3rd order tensor, where $x^l \in R^{M_l N_l K_d}$, where M is the height and N is the width and there are three channels; red, green, and blue, in this case $M = 256, N = 256$. Each element is designated by the index $(i; j; d)$, where $0 \leq i < M, 0 \leq j < N$ and $0 \leq d < 3$.

Convolutional layer. In this layer w^l multiple kernels and convolutions are used.

The kernel is assumed as K and each MxN kernel used is denoted as f, where f is a fourth order tensor$R^{MNk^l k}$ and the index variable $0 \leq i < M, 0 \leq j < N, 0 \leq d^l < K^1$ y $0 \leq d < K$ are used to indicate the element of the nucleus.

Stride is the kernel step that the image will go through, where its value $s = 1$. The convolution process is expressed as:

$$y_{i^l, j^{l+1}, d} = \sum_{i=0}^{M} \sum_{j=0}^{N} \sum_{d^l=0}^{d^l} f_{i,j,d^l,d} \times x^l_{i^{l+1}+i, j^{l+1}+j, d^l} + b_k \tag{1}$$

Where the bias is the constant b_k which is added to the equation with the value of1 ReLU layer. It is the activation function; it is denoted by:

$$y_{i,j,d} = \left(0, x^l_{i,j,d}\right) \tag{2}$$

Where $0 \leq i^{l+1} < M^l = M^{l+1}, 0 \leq j < N^1 = N^{l+1}$ and $0 \leq d < K^l = K^{l+1}$.

Pooling layer. Provides a reduced operation; reduces the in-plane dimensionality of feature maps. It generates another output vector, and the function is denoted by:

$$max : y_{i^{l+1},j^{l+1},d} = \ max \ x^l_{i^{l+1}\times M+i,j^{l+1}\times N+j,d^l} \tag{3}$$

$$0 < i < M, 0 < i < N \tag{4}$$

Where $0 \leq i^{l+1} < M^{l+1}$, $J^{l+1} < W^{l+1}$,y $0 \leq d < K^{l+1} = K^1$

Usually, the square size filter is established with size $f = 2$

Fully connected layer. It is a layer that lies between the convolutional layer and the output layer, each element in the input layer with each element in the output layer0.

Output layer. The Softmax function is applied connecting to the output layer. It contains the number of neurons classified. The logical function of r-dimensioning (z) with value between $[0; 1]$.

$$\sigma : R^r \to [0,1]^r \qquad \sigma\,(z) = \frac{e^{zj}}{\sum_{r=1}^{r} e^{z_r}} for\ j = 1, \ldots, r \tag{5}$$

Where z is the input to the output layer and r is the dimension of the vector z and j are the indices of the output unit [23].

SVM (Support Vector Machine) represents a multidimensional data set in a space where a hyperplane separates data elements belonging to different classes. The separating hyperplane is also called the optimal hyperplane. The SVM classifier can minimize generalisation errors on invisible data, it is trained with new features generated from training images. Finally, the trained SVM classifier recognises the classes [21].

For the training of the network, the images were used is $256x256$, the size of the batch size was4and the value of the learning rate was 0.00001, for the loss function the Adam optimiser was used [24].

Table 2 shows the configuration of the proposed network, considering that the layers in this case are 13, the first has an image resolution of $256x256$ and the convolution is 80 with the kernel size of 3 and the second has the same input size, with a convolution of 70 and kernel of 3 and so on until a series of dropout functions that serves to turn off or on functions, max-pooling to stay only with more important features. We also performed the flattening of the fully connected network and the softmax classification function with a total of 6 patterns.

In order to test the performance of the proposed network, the following CNNs have also been trained on the same set of data: VGG16 is a 16-layer convolutional neural network trained on the ImageNet dataset developed by Karen Simonyan and Andrew Zisserman of Oxford University in 2014 [25].

ResNet50 With a depth of 50 layers, it was presented by Kaiming He, Xiangyu Zhang, Shaoqing Ren and Jian Sun in 2015. The ResNet50 architecture was proposed to solve the leakage/explosion gradient problem by allowing the network to adapt to the residual mapping, rather than having the layers learn the underlying mapping. It uses a technique called skip connections, which allows the training of some layers to be skipped and connected directly to the output [26] InceptionV3 has a total of 42 layers and was presented by Simonyan Karen and Andrew Zisserman in 2015 [27] .

Layer	OutputShape	Parameter	
Conv1	(256, 256, 80, stride 3)	2240	
Conv2	(256,256,70)	3	50470
Conv3	(256,256,60)	37860	
Conv4	(254,254,50)	27050	
Conv5	(254,254,28)	12628	
Maxpooling	(127,127,28)		
Conv6	(127,127,64)	16192	
Conv (7,8,9)	(127,127,32)	18464	
Maxpooling	(63,63,32)		
Conv10	(63,63,64)	18496	
Conv(11,12,13)	(63,63,32)	9248	
Dropout	(63,63,32)		
Maxpooling	(31,31,32)		
Flatten	(30752)		
Fully connected	(5000)		
Dropout,	5000		
SVM			
Softmax	6	1005	

Table 2: Proposed network configuration

4 Results and discusión

To test the performance of each CNN network, a sample of 45 test images was predicted using the confusion matrix, obtaining the parameters TP = true positive; TN = true negative; FP = false positive; FN = false negative. Confusion matrix results for (a) our proposed method, (b) InceptionV3, (c) VGG16, and (d) ResNet50 are shown in Figure 4.

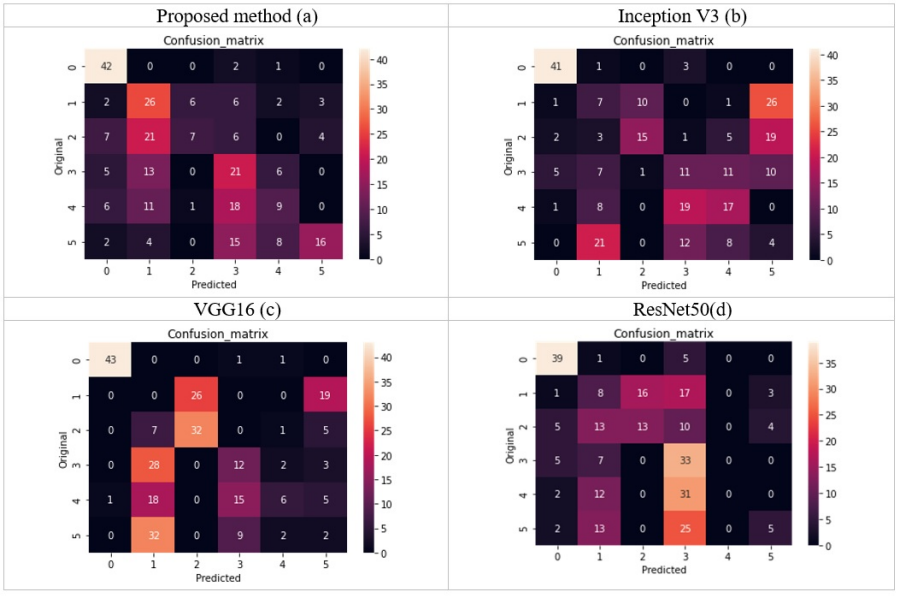

Figure 4: The confusion matrix of each trained Architecture

Exactitud o *Acurracy* Es igual a la proporción de predicciones que el modelo clasifico correctamente.

$$Accuracy = \frac{TP + TN}{TP + TN + FP + FN} \tag{6}$$

Precisión Es el valor predictivo positivo

$$Precision = \frac{TP}{TP + FP} \tag{7}$$

Especificidad o *Recall* Mide la proporción de negativos reales que se identifican correctamente

$$Recall = \frac{TP}{TP + FN} \tag{8}$$

F1-score Es una medida de precisión y recuperación, puede tener una puntuación máxima de 1 o mínima de 0.

$$Precision = \frac{2TP}{2TP + FP + FN} \tag{9}$$

Table 3 shows the results obtained from the confusion matrix of our proposal and the ResNet50, VGG16 and InceptionV3 architectures, of which the proposed method obtained the best accuracy with 0.45, followed by the VGG16 models with 0.35, Inception V3 with 0.35 and finally the ResNet50 network with 0.24. It is worth noting that the accuracy results are low because the classes are confused by others, which is not surprising since each class has one more pattern added to it, causing greater confusion between classes.

Arquitectures	*Accuracy*	*Precision*	*Recall*	*F1-score*
Our proposed method	0.45	0.48	0.45	0.42
InceptionV3	0.35	0.38	0.35	0.36
Vgg16	0.35	0.40	0.35	0.36
ResNet50	0.24	0.20	0.24	0.18

Table 3: Results of the confusion matrix

The ROC curve is an average of the classification performance; if the AUC is equal to 1, the classifier achieves perfect accuracy [29].

$$AUC\left(f\right) = Pr\left(f\left(x^{+}\right) > f\left(x^{-}\right)\right) \tag{10}$$

To know the fit of the data and to improve the results, the following kernels were used: Linear, Gaussian, RBF, Sigmoid, Polynomial, with the SVM [30, 31]. After classification with the SVM, the ROC curve and AUC are estimated.

Figure 5 shows the comparative ROC curves with the best performing kernels. The best architectures with ROC curves were with the proposed method and InceptionV3, giving a macro average of 0.80 respectively.

It should be noted that the ResNet50 architecture could not classify class 4, so class 4 is not shown.

There could be a lot of confusion between classes one with five and four, or between classes four and three, because of the types of tuberculosis patterns that occur in each of the classes. This suggests that ResNet50 has a lot of confusion between the classes, such that it could not recognise class four. This can be seen in the confusion matrix of ResNet50, on the other hand, despite the low accuracy of the training, the ROC curves

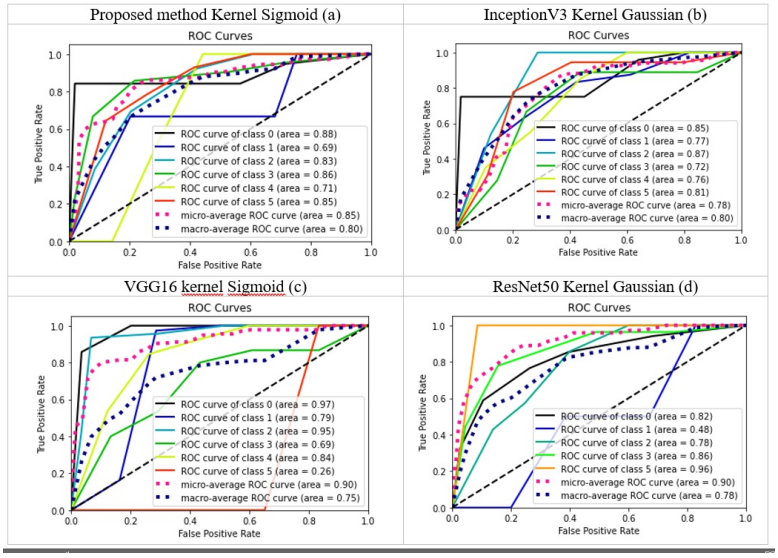

Figure 5: ROC curves of the proposed method, Inception architecture V3, VGG16 and ResNet50

showed that the models were able to achieve a micro-average above 0.78.

Table 4 the kernels used and the macro average of each CNN architecture, highlighting the best kernel of each architecture, equating our proposed architecture with the sigmoidal kernel and Inception V3 with the Gaussian kernel, both with a micro average of 0.80.

Kernel	*Proposed method*	*Inception V3*	*VGG16*	*ResNet50*
Linear	0.74	0.62	0.68	0.61
Gaussian	0.73	0.80	0.71	0.78
RFB	0.77	0.69	0.65	0.72
Sigmoid	0.80	0.69	0.75	0.59
Polynomial	0.59	0.46	0.59	0.70

Table 4: Results of the confusion matrix

A comparison of the state-of-the-art results is shown in Figure 6.

5 Conclusions

In the radiographs of patients with tuberculosis, more than one type of tuberculosis pattern can be detected at the same time, so it is strongly recommended that future studies consider the presence of more than one type of tuberculosis and not only one. The studies found only consider a single type of tuberculosis. In this sense, this work is pioneering.

The article proposes a classifier of tuberculosis patterns present in the same patient in chest radiographs. The patterns detected are fibrosis, opacity, nodules, cavitations, pleural and consolidation, which increases the degree of difficulty in this research. The proposed method presents good results, the other investigations only consider one pattern.

The contrasting of results were performed with four CNN architectures; the first was the proposed architecture, the second with InceptionV3, both showed good results, the third was the VGG16 architecture and finally

	Y. Xie *et al* RCNN [14]	Y. Xie *et al* FPN [14]	Y. Xie *et al* [14]	Becker *et al.* [13] ROC	ResNet-50 ROC	VGG16 ROC	Inception V3 ROC	ProM ROC
Exudation	41.49	50.96	53.74	-	-			-
Calcification	5.52	42.84	41.82	-	-			-
Nodule	0.37	17.50	22.73	-	-			-
Miliary	40.57	87.72	84.62	0.83	-			-
Free Pleural Effusion	45.65	52.67	64.92	1.0	-			-
Encapsulated Pleural Effusion	2.36	52.13	52.79	-	-			-
Cavity	-	-	-	0.90	-			-
Consolidation	-	-	-	0.75	-			-
Intestinal	-	-	-	0.78	-			-
Healthy	-	-	-	-	0.82	0.97	0.85	0.88
Consolidation and opacity	-	-	-	-	0.78	0.95	0.87	0.83
Fibrosis, opacity and nodules	-	-	-	-	0.86	0.69	0.72	0.86
Consolidation, fibrosis, opacity and nodules	-	-	-	-	0	0.84	0.76	0.71
Consolidation, fibrosis, opacity, nodules and cavitations	-	-	-	-	0.96	0.26	0.81	0.85
Consolidation, fibrosis, opacity, pleural, nodules and cavitations	-	-	-	-	0.48	0.79	0.77	0.69

Figure 6: Comparison of results with the literature.

the ResNet-50 architecture which did not perform well in the classification of four patterns.

To validate the results, we used the ROC curve and AUC with 5 types of kernels (Linear, Gaussian, Polynomial, Sigmoid and RBF), the best result obtained for our proposal was the Sigmoid kernel and for the InceptionV3 network was the Gaussian kernel; both with an AUC of 0.80%.

Convolutional networks perform well in feature retrieval, but in association with support vector machines they substantially improve classification, as other research has also shown.

This work is relevant since no other research was found that considers the presence of more than one tuberculosis pattern in the same patient.

It is advisable to continue collecting more data, to carry out this type of research, so it would be advisable to create a larger database for further research.

It is considered that future work can be done to improve the accuracies, one research opportunity is to consider transfer of learning; a technique that has shown to improve the results in other works where work is done with CNC. Another research opportunity is to work with segmented lungs, to avoid the noise caused by the bone structure.

It would also be possible to work with tomography images since they integrate images with several angles of the lungs.

6 Recognition

The authors would like to thank the Universidad Autónoma del Estado de México for supporting this work. Also, this research work was sponsored by the Consejo Nacional de Ciencia y Tecnología (CONACyT) with the National grant, folio 764877.

We would like to thank the National Institute of Allergy and Infectious Diseases (NIAID) TB Portals DEPOT laboratory for their collaboration. They provided the images duly diagnosed and described, without their collaboration this work would not have been possible.

References

[1] A. Castiñeira Estévez, M. López Pedreira, M. Pena Rodríguez, and M. Liñares Iglesias, "Medicina preventiva y asistencial en el medio rural.," Medicina Integral. Accessed: Oct. 11, 2021. [Online]. Available: https://www.elsevier.es/es-revista-medicina-integral-63-pdf-13029945

[2] R. Garza-Velasco, J. Ávila-de Jesús, and L. M. Perea-Mejía, "Tuberculosis pulmonar: la epidemia mundial continúa y la enseñanza de este tema resulta crucial y compleja," Educación Química, vol. 28, no. 1, Jan. 2017, doi: https://doi.org/10.1016/j.eq.2016.09.009

[3] Geneva: World Health Organization, "Global tuberculosis report 2023," Oct. 2023. Accessed: Dec. 06, 2023. [Online]. Available: https://www.who.int/teams/global-tuberculosis-programme/tb-reports

[4] Newsroom World Health Organization, "Tuberculosis." Accessed: Dec. 06, 2023. [Online]. Available: https://www.who.int//news-room/fact-sheets/detail/tuberculosis/?gad_source=1&gclid=CjwKCAjwkJm0BhBxEiwAwT1AXAqTDpJAh8TE6QYBd1L4B1-kYdX6tBW7QHcfyUKlJBmoC_nU8xgqABoCr0cQAvD_BwE

[5] Geneva: World Health Organization, "Global strategy for tuberculosis research and innovation." [Online]. Available: https://www.who.int/es/publications/i/item/9789240010017 .

[6] A. M. Ismael and A. Şengür, "Deep learning approaches for COVID-19 detection based on chest X-ray images," Expert Syst Appl, vol. 164, Feb. 2021, doi:https://doi.org/10.1016/j.eswa.2020.114054.

[7] S. Stirenko et al., "Chest X-Ray Analysis of Tuberculosis by Deep Learning with Segmentation and Augmentation," in 2018 IEEE 38th International Conference on Electronics and Nanotechnology (ELNANO), IEEE, Apr. 2018. doi: https://doi.org/10.1109/ELNANO.2018.8477564

[8] T. Karnkawinpong and Y. Limpiyakorn, "Classification of pulmonary tuberculosis lesion with convolutional neural networks," J Phys Conf Ser, vol. 1195, Apr. 2019, doi: https://doi.org/10.1088/1742-6596/1195/1/012007 .

[9] National Institute of Health, "NIAID TB PORTALS DEPOT." Accessed: Mar. 06, 2021. [Online]. Available: https://depot.tbportals.niaid.nih.gov/#/home

[10] S. Rajaraman and S. K. Antani, "Modality-Specific Deep Learning Model Ensembles Toward Improving TB Detection in Chest Radiographs," IEEE Access, vol. 8, 2020, doi: https://doi.org/10.1109/ACCESS.2020.2971257

[11] A. H. Al-Timemy, R. N. Khushaba, Z. M. Mosa, and J. Escudero, "An Efficient Mixture of Deep and Machine Learning Models for COVID-19 and Tuberculosis Detection Using X-Ray Images in Resource Limited Settings," pp. 77–100, Jul. 2021, doi: https://doi.org/10.1007/978-3-030-69744-0_6

[12] P. Lakhani and B. Sundaram, "Deep Learning at Chest Radiography: Automated Classification of Pulmonary Tuberculosis by Using Convolutional Neural Networks," Radiology, vol. 284, no. 2, Aug. 2017, doi:https://doi.org/10.1148/radiol.2017162326

[13] A. S. Becker et al., "Detection of tuberculosis patterns in digital photographs of chest X-ray images using Deep Learning: feasibility study," The International Journal of Tuberculosis and Lung Disease, vol. 22, no. 3, Mar. 2018, doi: https://doi.org/10.5588/ijtld.17.0520

[14] Y. Xie et al., "Computer-Aided System for the Detection of Multicategory Pulmonary Tuberculosis in Radiographs," J Healthc Eng, vol. 2020, pp. 1–12, Aug. 2020, doi: https://doi.org/10.1155/2020/9205082.

[15] W. H. Curioso and M. J. Brunette, "Inteligencia artificial e innovación para optimizar el proceso de diagnóstico de la tuberculosis," Rev Peru Med Exp Salud Publica, vol. 37, no. 3, Sep. 2020, doi: https://doi.org/10.17843/rpmesp.2020.373.5585.

[16] S. I. Nafisah and G. Muhammad, "Tuberculosis detection in chest radiograph using convolutional neural network architecture and explainable artificial intelligence," Neural Comput Appl, vol. 36, no. 1, pp. 111–131, Jan. 2024, doi: https://doi.org/10.1007/s00521-022-07258-6.

[17] A. Iqbal, M. Usman, and Z. Ahmed, "Tuberculosis chest X-ray detection using CNN-based hybrid segmentation and classification approach," Biomed Signal Process Control, vol. 84, p. 104667, Jul. 2023, doi: https://doi.org/10.1016/j.bspc.2023.104667.

[18] Goswami K K, Kumar R, Kumar R, Akshay J. Reddy, Goswami.S. K. "Deep Learning Classification of Tuberculosis Chest X-rays". Cureus 15(7): e41583. July 08, 2023. doi: https://doi.org/10.7759/cureus.41583

[19] Escorcia-Gutierrez J, Soto-Diaz R, Madera N., Burgos-Florez F., Rodríguez A., Soto C., and Mansour R.F "Computer Aided Diagnosis for Tuberculosis Classification with Water Strider Optimization Algorithm". Computer Systems Science Engineering. CSSE, 2023, vol.46, no.2. doi: https://doi.org/10.32604/csse.2023.035253.

[20] A. K. Baszczyńska, "Empirical and Kernel Estimation of the ROC Curve," Acta Universitatis Lodziensis. Folia Oeconomica, vol. 1, no. 311, Apr. 2015, doi: https://doi.org/10.18778/0208-6018.311.06.

[21] S. Ahlawat and A. Choudhary, "Hybrid CNN-SVM Classifier for Handwritten Digit Recognition," Procedia Comput Sci, vol. 167, 2020, doi: https://doi.org/10.1016/j.procs.2020.03.309.

[22] J. Wu, "Introduction to Convolutional Neural Networks." [Online]. Available: https://api.semanticscholar.org/CorpusID:36074296

[23] B. Triwijoyo, B. Sabarguna, W. Budiharto, and E. Abdurachman, "ICIC Express Letters ICIC International 2020 ISSN," ICIC Express Letters, vol. 14, pp. 635–641, Oct. 2020, doi: https://doi.org/10.24507/icicel.14.07.635.

[24] D. P. Kingma and J. Ba, "Adam: A Method for Stochastic Optimization," Dec. 2014. doi: https://doi.org/10.48550/arXiv.1412.6980

[25] K. Simonyan and A. Zisserman, "Very Deep Convolutional Networks for Large-Scale Image Recognition," Sep. 2014.

[26] K. He, X. Zhang, S. Ren, and J. Sun, "Deep Residual Learning for Image Recognition," Dec. 2015. doi: https://doi.org/10.48550/arXiv.1512.03385

[27] C. Szegedy, V. Vanhoucke, S. Ioffe, J. Shlens, and Z. Wojna, "Rethinking the Inception Architecture for Computer Vision," Dec. 2015. https://doi.org/10.48550/arXiv.1512.00567

[28] S. Visa, B. Ramsay, A. Ralescu, and E. Knaap, "Confusion Matrix-based Feature Selection.," in CEUR Workshop Proceedings, Oct. 2011, pp. 120–127. [Online]. Available: https://api.semanticscholar.org/CorpusID:3026044

[29] Y. Tian, Y. Shi, X. Chen, and W. Chen, "AUC Maximizing Support Vector Machines with Feature Selection," Procedia Comput Sci, vol. 4, 2011, doi: https://doi.org/10.1016/j.procs.2011.04.183

[30] I. Roman, R. Santana, A. Mendiburu, and J. A. Lozano, "In-depth analysis of SVM kernel learning and its components," Neural Comput Appl, vol. 33, no. 12, Jun. 2021, doi: https://doi.org/10.1007/s00521-020-05419-z.

[31] M. Achirul Nanda, K. Boro Seminar, D. Nandika, and A. Maddu, "A Comparison Study of Kernel Functions in the Support Vector Machine and Its Application for Termite Detection," Information, vol. 9, no. 1, p. 5, Jan. 2018, doi: https://doi.org/10.3390/info9010005.